Off-Axis Temperature Anisotropy Measurement by Double-Pass Thomson Scattering Diagnostic System on TST-2*)

Junichi HIRATSUKA, Akira EJIRI, Makoto HASEGAWA[1)], Yoshihiko NAGASHIMA[1)], Yuichi TAKASE, Hiroshi TOJO[2)], Takashi YAMAGUCHI, Takanori AMBO, Hirokazu FURUI, Takahiro HASHIMOTO, Hidetoshi KAKUDA, Kunihiko KATO, Takuya OOSAKO, Takuya SAKAMOTO, Ryota SHINO, Takahiro SHINYA, Masateru SONEHARA, Takuma WAKATSUKI and Osamu WATANABE

The University of Tokyo, Kashiwa 277-8561, Japan
[1)]*Kyushu University, 6-1 Kasuga-koen, Kasuga, Fukuoka 816-8580, Japan*
[2)]*Japan Atomic Energy Agency, 801-1 Mukoyama, Naka-shi, Ibaraki 311-0193, Japan*

(Received 2 December 2011 / Accepted 24 April 2012)

We have developed a multi-point Thomson scattering system with double-pass configuration for the TST-2 device and have installed new collection optics for the same. Temperature and density can now be measured simultaneously at four points by using four fibers and four polychromators. Herein, we present results of off-axis temperature anisotropy measurements performed with this system, in which no temperature anisotropy beyond the error bar was observed for ohmic plasmas.

Keywords: Thomson scattering, double-pass configuration, temperature anisotropy, multi-point diagnostics, TST-2

DOI: 10.1585/pfr.7.2402092

1. Introduction

Diagnostics of density and temperature by Thomson scattering is important for understanding low-density plasma, such as a non-inductive spherical tokamak (ST) plasma, which has an electron density of $n_e \simeq 10^{17}$ to 10^{18} m^{-3}. The Thomson scattering signal, however, is very weak for such low-density plasmas, whereas laser power is limited. Therefore, amplification by a multipass scheme is effective. For example, the total probe energy of Thomson-scattered light was amplified 90-fold in TEXTOR [1] using a multipass intra-cavity configuration. The multipass configuration, including the double-pass configuration, is attractive because it offers the possibility of temperature anisotropy measurements. At the Thomson scattering system in the Tokyo Spherical Tokamak 2 (TST-2) device, backward and forward Thomson-scattered light are measured via a double-pass configuration. In this case, the temperature anisotropy can be measured directly depending on the angle between $\vec{k}_i - \vec{k}_s \equiv \Delta\vec{k}$ and the magnetic field, where $\vec{k}_i$ denotes the incident wave vector of the laser irradiation and $\vec{k}_s$ denotes the scattered wave vector [2]. Temperature anisotropy may appear in low-density collisionless ST plasmas because of the large mirror effect. Although temperature anisotropy is important in equilibrium and transport, no method has been developed to directly measure it.

As a pilot experiment of multipass, we developed a double-pass Thomson scattering configuration and applied it to the measurement of the plasma center temperature anisotropy [3]. With an appropriate double-pass configuration such as that in the TST-2 Thomson scattering system, the direction of $\Delta\vec{k}$ is differing between the first and second pass and temperatures corresponding to each direction can be measured by signals from each pass. For isotropic-temperature plasmas, this scheme provides a highly reliable measurement of temperature and density because temperature and density are measured twice at almost the same spatial and temporal location (in TST-2, the differences are about 10 mm and 30 to 40 ns, respectively). In addition, the width of Doppler broadening differs for different $\left|\Delta\vec{k}\right|$ and calibration error may easily be detected. We applied a single-spatial-point Thomson scattering system in double-pass configuration to an isotropic ohmic plasma ($n_e \simeq 10^{19}$ m^{-3}) in TST-2 and confirmed that the temperature anisotropy measurement is feasible with 10% error [3].

Although the ohmic plasma density is high, there can be a collisionless regime and, provided the magnetic momentum is conserved, electron thermal velocities can be observed as $v_{e,\parallel} \ll v_{e,\perp}$ on the high-field-side (HFS) and $v_{e,\parallel} \gg v_{e,\perp}$ on the low-field-side (LFS). The difference becomes clearer near the edge, where the mirror ratio becomes as large as five for the low-aspect-ratio ST plasmas in TST-2. To search for such off-axis temperature anisotropy, we installed new collection optics and devel-

author's e-mail: hiratsuka@fusion.k.u-tokyo.ac.jp
*) This article is based on the presentation at the 21st International Toki Conference (ITC21).

oped a multipoint Thomson scattering diagnostic system, which we described in the first part of this paper.

The angle between $\Delta\vec{k}$ and the magnetic field, $\vec{B}$, is important for temperature anisotropy measurements and varies along the measurement points. The quality of temperature anisotropy measurements is limited by this angle. In the second part of this paper, this limitation is described assuming that the electron velocity distribution is bi-Maxwellian with two components: one perpendicular and one parallel to the magnetic field (i.e., $T_{e,\perp}$ and $T_{e,\parallel}$).

To precisely measure electron temperature, it is essential to precisely calibrate the relative sensitivity of each polychromator wavelength channel, which is performed using light from a monochromator. In addition, a standard light was used to directly calibrate each polychromator channel and measure the efficiency of the collection optics for the Thomson scattering system. However, when using a continuous wave (cw) standard light, the voltage drop at the protection resistance in the detection circuit may become a problem. Herein, we describe a method that overcomes this difficulty and uses cw light to directly calibrate and correct the sensitivity reduction.

We measured the electron temperature profile and the electron-temperature anisotropy profile for an ohmic plasma in TST-2 using a double-pass multipoint Thomson scattering system. To date, the measured temperature anisotropy remains within the error bar.

2. Double-Pass Multipoint Thomson Scattering Diagnostic System

A compact and bright double-pass [3] Thomson scattering diagnostic system has been developed in TST-2 [4, 5]. The specifications of the Nd:YAG laser are as follows: energy (1.6 J), repetition frequency (10 Hz), and pulse width (10 ns). The system uses polychromators with six wavelength channels with the acceptance of each channel center determined by interference filters having center wavelengths of 980, 1020, 1040, 1050, 1055, and 1059 nm. The throughput of each channel is detected by an avalanche photo diode (APD). A spherical mirror reflects the laser pulse so that the pulse traverses the plasma in the forward and backward directions, and the corresponding scattered pulses are separated by 30 to 40 ns and have a full width at half maximum of 10 ns. To distinguish between these two Thomson-scattered light pulses, a fast low-noise detection circuit was developed and installed in the polychromator [6]. A fiber with large numerical-aperture (N.A. = 0.37) contributes to very efficient measurements.

To achieve multipoint diagnostics, we installed new collection optics that consist of 600-mm-diameter spherical mirror of 300 mm focal length to collect the light and focus it into a set of optical fibers positioned by a specially designed fiber holder (see Fig. 1). This setup allows us to measure the range of 240 mm $< R <$ 540 mm, where R denotes the major radius. The design (i.e., calculated) value

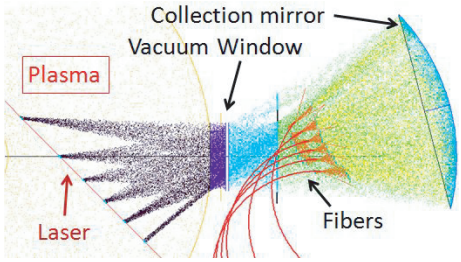

Fig. 1 Ray tracing result for collection optics.

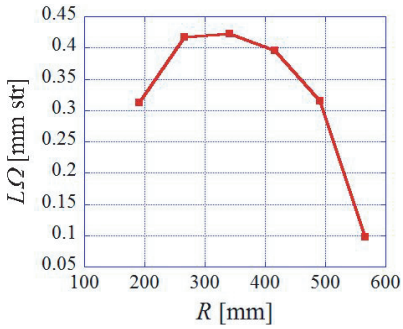

Fig. 2 Design value of $L\Omega$.

of $L\Omega$ is shown in Fig. 2 , in which L denotes the scattering length and Ω denotes the scattering solid angle. Currently four spatial points are measured simultaneously by using four fibers and four polychromators.

In the standard procedure, the calibration is performed by using a standard light and monochromator. However, relative sensitivity depends on environmental temperature and optical conditions, such as the incident angle of the light, the scattering solid angle, and the reflectivity of the collection mirror. Therefore, direct sensitivity calibration under the same conditions result in more precise measurements. For TST-2, we calibrate the relative sensitivity using a standard light and plane mirror in the same environment and with the same collection optics. In this procedure, a plane mirror is positioned at the vacuum window (see Fig. 1) and a standard light (with a diffuser panel) is positioned conjugate to the scattering point. With this setup, the incident angle of the light, the scattering solid angle of the standard light scattered into the fiber by the diffuser, and the reflectivity of the collection mirror are almost identical as for the Thomson scattering measurement.

A cw standard light is used for this calibration. In the detector circuit, a protection resistance (1 MΩ) is inserted in series with the APD. When the APD current is induced by the cw light, the APD bias voltage drops. Because the APD amplification depends on bias voltage, this drop reduces the APD sensitivity. Conversely, a capacitor inserted in parallel with the APDs makes the voltage drop negligible for short-time ohmic plasma (100 ms). Thus, this sensitivity reduction induced by cw calibration light must be corrected. From some test calibrations, we found that the

relative sensitivity of each channel was reduced by 1% for output voltages as large as 29.0 mV. The relative sensitivity of the polychromator is corrected based on this result.

3. Quality of Temperature Anisotropy Measurement

The angle ($\equiv \delta$) between $\Delta\vec{k}$ and the magnetic field, $\vec{B}$, depends on the measurement point. Because the magnetic field consists of the toroidal field and the poloidal field, δ is expressed as

$$\delta = \cos^{-1}\left(\cos\left(\theta\right)\cos\left(\phi\right)\right), \tag{1}$$

where θ and ϕ denote the pitch angle and the angle between $\Delta\vec{k}$ and the toroidal magnetic field B_t, respectively (see Fig. 3). The radial profile of δ for a typical discharge is shown in Fig. 4. When $\delta = 90°$, the temperature perpendicular to the magnetic field is measured, and when $\delta = 0°$, the temperature parallel to the magnetic field is measured. When the plasma center ($R \simeq 373$ mm) is measured, $T_{e,\perp}$ and $T_{e,\parallel}$ are obtained from the backward and the forward scattering, respectively. In other areas, however, the effects of $T_{e,\perp}$ and $T_{e,\parallel}$ are mixed, and we differentiate between these two contributions by the following analysis:

Assuming that the electron velocity distribution function, f_e, is bi-Maxwellian, f_e is expressed as

$$f_e\left(v_{e,\perp}, v_{e,\parallel}\right) = n_e f_{e,\perp} f_{e,\parallel}, \tag{2}$$

where n_e denotes electron density. The quantities, $f_{e,\perp}$ and $f_{e,\parallel}$ are the normalized electron velocity distribution functions with components purely perpendicular and purely parallel to the magnetic field, respectively, and are defined as

$$f_{e,\perp}\left(\boldsymbol{v}_{e,\perp}\right) = \frac{m_e}{2\pi T_{e,\perp}} \exp\left(-\frac{m_e}{2}\frac{\boldsymbol{v}_{e,\perp}^2}{T_{e,\perp}}\right), \tag{3}$$

$$f_{e,\parallel}\left(v_{e,\parallel}\right) = \sqrt{\frac{m_e}{2\pi T_{e,\parallel}}} \exp\left(-\frac{m_e}{2}\frac{v_{e,\parallel}^2}{T_{e,\parallel}}\right), \tag{4}$$

where m_e denotes electron mass and $\boldsymbol{v}_{e,\perp}$ and $v_{e,\parallel}$ denote the components of the electron velocity perpendicular and parallel to the magnetic field, respectively. For $\delta = \delta_{first}$ for the first pass, f_e with $|\boldsymbol{v}_{e,\perp}| = v_e \sin(\delta_{first})$ and $v_{e,\parallel} = v_e \cos(\delta_{first})$ are measured from the first pass. In this case, the effective temperature $T_{e,first}^{eff}$ from the first pass is given as

$$\frac{1}{T_{e,first}^{eff}} = \frac{\sin^2(\delta_{first})}{T_{e,\perp}} + \frac{\cos^2(\delta_{first})}{T_{e,\parallel}}. \tag{5}$$

The relationship between the measured, $T_{e,first}^{eff}$ and the pure perpendicular and parallel components of temperature are given by Eq. (5). Thus, the effective temperature anisotropy is expressed as

$$\frac{T_{e,first}^{eff} - T_{e,second}^{eff}}{T_{e,first}^{eff}} = 1 - \frac{\cos^2(\delta_{first}) + (T_{e,\parallel}/T_{e,\perp})\sin^2(\delta_{first})}{\cos^2(\delta_{second}) + (T_{e,\parallel}/T_{e,\perp})\sin^2(\delta_{second})}. \tag{6}$$

Figure 4 shows the radial profile of $\left(T_{e,first}^{eff} - T_{e,second}^{eff}\right)/T_{e,first}^{eff}$, assuming a 10% temperature anisotropy (i.e., $T_{e,\parallel}/T_{e,\perp} = 1.1$).

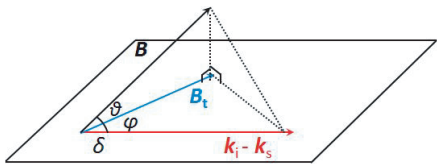

Fig. 3 Definition of angles θ, ϕ and δ.

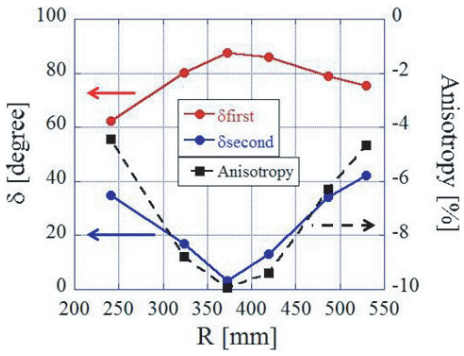

Fig. 4 Angle δ of the first- (red) and the second- (blue) pass at each position. Black symbols denote electron temperature anisotropy to be measured when there is a 10% anisotropy at each position.

4. Temperature Profile from Double-Pass Multipoint Measurement

We applied the double-pass multipoint Thomson scattering diagnostic system to TST-2 ohmic plasmas. To increase the signal-to-noise ratio, a high-density plasma was produced. Three typical plasma-discharge waveforms are shown in Fig. 5, and Fig. 6 shows a typical plasma temperature profile measured by the double-pass multipoint system. Because we can simultaneously measure four spatial points, we obtained the profile from the three similar discharges shown in Fig. 5. In Fig. 6, red symbols denote first-pass measurements, and blue symbols denote second-pass measurements. The first- and the second-pass measurement points were separated by about 10 mm. The inboard limiter and outboard limiter were located at $R = 130$ and 585 mm, respectively. A flat temperature profile forms over a wide region (260 mm $< R <$ 500 mm). Figure 7 shows the relative error dependence as a function of detected photon number, in which N is the photon number detected in one wavelength channel of the polychromator and $\delta N/N$ is the relative error in N. From Fig. 7, we observe that $\delta N/N$ is inversely proportional to N. Because

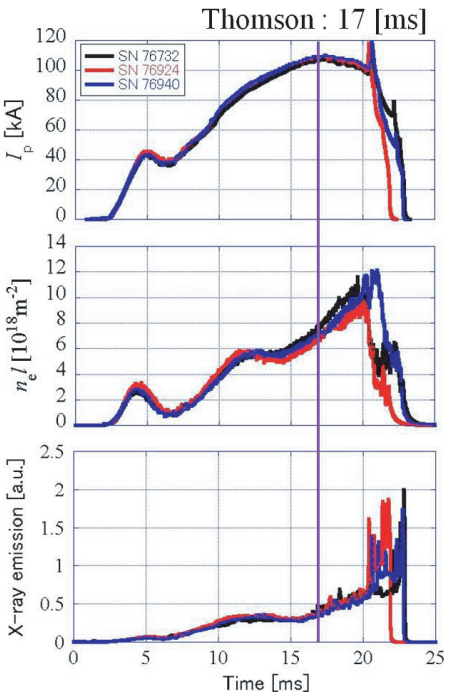

Fig. 5 Typical waveforms of plasma discharge. The x-ray emission is for energies ranging from 7 to 6000 eV. Electron temperature and temperature anisotropy of these discharges are shown in Fig. 6.

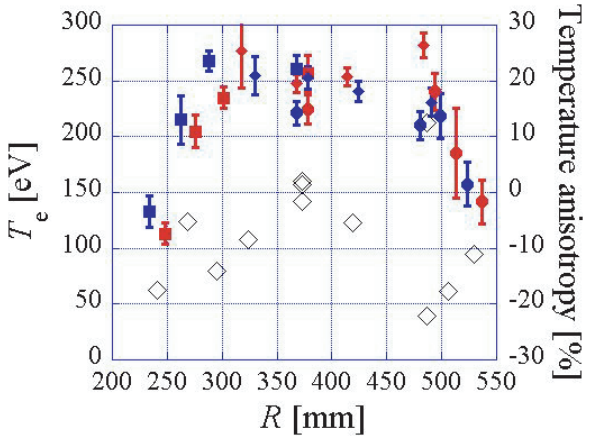

Fig. 6 Temperature profile obtained from three similar ohmic plasmas. First-pass measurements are in red and second-pass measurements are in blue. Different symbols denote the results of different discharges. Black diamonds denote the electron temperature anisotropy $\left|\left(T^{\rm eff}_{\rm e,first} - T^{\rm eff}_{\rm e,second}\right)/T^{\rm eff}_{\rm e,first}\right|$.

the error of T_e is proportional to $\delta N/N$; the error of T_e, under the present conditions, is independent of the number of detected photons. There is a 10% error in temperature over the range 260 mm $< R <$ 430 mm, and the error is large at $R >$ 480 mm (typically 30%), which suggests that the electron density is low in this area.

Figure 8 shows the relationships between the temperatures evaluated by the first and the second passes. The quantity R denotes the center of the measurement points between the first and the second passes. $T_{\rm e,first}$ denotes the temperature evaluated by the first pass and $T_{\rm e,second}$ denotes the temperature evaluated by the second pass. The values of $\langle(T_{\rm e,first} - T_{\rm e,second})/T_{\rm e,first}\rangle$ at R = 324, 373, 419, and 487 mm are −4.70% ± 8.04%, −2.55% ± 10.5%, −0.414% ± 10.3% and −14.5% ± 22.2%, respectively. Therefore, there is no temperature anisotropy beyond the error bar. Note that the error bar is determined according to

$$\sqrt{\frac{1}{N}\sum^{N}\left(\frac{T_{\rm e,first} - T_{\rm e,second}}{T_{\rm e,first}}\right)^2}, \qquad (7)$$

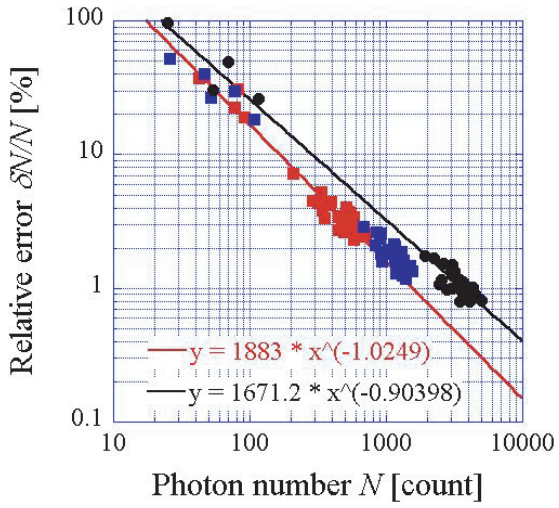

Fig. 7 Relationship between N and $\delta N/N$. Red and blue symbols denote the same channel (central transmittance wavelength of 1050 nm) in the first- and second-pass, respectively. Black symbols denote a channel (central transmittance wavelength of 1020 nm) in which the largest number of photons are detected in the first-pass.

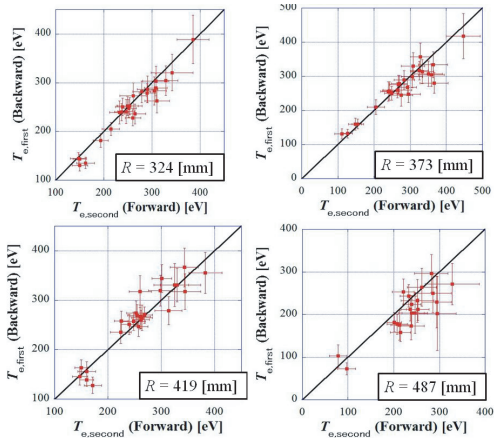

Fig. 8 Relationship between temperatures measured by first- and second-pass at four positions with error bars (red). Black lines show isotropic case.

where N denotes the number of data. Here, we describe the two possible causes of the finite average value of anisotropy. The first candidate is pure plasma temperature anisotropy. The measured anisotropy is reduced compared with the pure anisotropy, depending on the angle δ. The accuracy of the anisotropy measurement should be less than 10% at the core and 4% at the edge when measuring 10% pure anisotropy (see Fig. 4). Because the present accuracy of the anisotropy measurement is insufficient, we must reduce the error. Electromagnetic noise from the laser could be the main source of error. The second candidate is the effect of a large temperature gradient. Because the measurement points of the first and second pass are separated by about 10 mm, the temperatures of the two points must differ when there is a large temperature gradient in the LFS or the HFS. For this reason, the distance between the two measurement points should be reduced in the double-pass configuration.

5. Summary and Future Work

After installing new collection optics, we constructed a double-pass multipoint Thomson scattering diagnostic system for TST-2. With this system, we measured a flat electron temperature profile and electron anisotropy profile for ohmic plasmas and found no significant anisotropy. To confirm this result, we need to identify and reduce the source of constant error. In addition, we plan to develop a multipass configuration to amplify the signal.

Acknowledgments

This work was supported by Japan Society for the Promotion of Science (JSPS) Grant-in-Aid for Scientific Research Nos. 21246137 and 21226021 and by the National Institute for Fusion Science (NIFS) Collaborative Research Program No. NIFS09KUTR039.

[1] M.Yu. Kantor *et al.*, Plasma Phys. Control. Fusion **51**, 055002 (2009).
[2] E. Yatsuka *et al.*, Nucl. Fusion **51**, 123004 (2011).
[3] J. Hiratsuka *et al.*, Plasma Fusion Res. **6**, 1202133 (2011).
[4] S. Kainaga *et al.*, Plasma Fusion Res. **3**, 027 (2008).
[5] T. Yamaguchi *et al.*, Plasma Fusion Res. **5**, S2092 (2010).
[6] A. Ejiri *et al.*, Plasma Fusion Res. **5**, S2082 (2010).